ELSEVIER

Materials Science and Engineering A 437 (2006) 379–387

MATERIALS SCIENCE & ENGINEERING A

www.elsevier.com/locate/msea

Strain and deformation in ultra-hard nanocomposites nc-TiN/a-BN under hydrostatic pressure

Stephen G. Prilliman [a,b], Simon M. Clark [c,*], A. Paul Alivisatos [a,b], Pavla Karvankova [d], Stan Vepřek [d]

[a] *Department of Chemistry, University of California at Berkeley, Berkeley, CA 94720, USA*
[b] *Materials Science Division, Lawrence Berkeley National Laboratory, Berkeley, CA 94720, USA*
[c] *Advanced Light Source, Lawrence Berkeley National Laboratory, Berkeley, CA 94720, USA*
[d] *Department of Chemistry, Technical University Munich, Lichtenbergstr. 4, D-85747 Garching, Germany*

Received 1 December 2005; received in revised form 24 July 2006; accepted 26 July 2006

Abstract

A high pressure diffraction study, from ambient to 50 GPa, has been carried out on nanocrystalline TiN/amorphous BN nanocomposite materials prepared by plasma chemical vapor deposition. The compressibilities of these materials were found not to be significantly different from TiN. A large amount of biaxial and isotropic strain was found to build up on pressurization which continued to exist after depressurization and annealing indicating a permanent deformation under high pressure. This permanent deformation is located in the grain boundaries and is reduced by the presence of amorphous BN.

Keywords: Titanium nitride; Superhard nanocomposites; Nanocryatalline; Composite; X-ray diffraction; Compressibility; High pressure

1. Introduction

The hardness or resistance to deformation upon indentation, of diamond is 70–100 GPa, the highest of any natural material. This is due to the high strength of the carbon–carbon bond and the three-dimensional support structure provided by its tetrahedral bonding geometry. Because of their hardness and thermal stability, diamond and diamond-coated tools can be used under conditions where other materials will fail. However, diamond has a number of practical limitations. It is costly and still rather difficult to deposit as thin coatings. It is impossible to use diamond for the machining of steel and other carbide forming metals because carbon alloys with these materials at high temperature. For this reason there has been much effort to discover new "ultra-hard" coatings that would have hardness on the order of diamond [1,2]. Considerable attention has been paid to thin films of transition metal nitrides, carbides and borides. Like diamond, these materials have a strong network of bonds and are thus inherently resistive to deformation.

While thin films of transition metal nitrides, borides and carbides have proven to be quite hard (hardness ≈ 20–30 GPa), their hardness can be greatly enhanced by preparing the films in such a way as to precipitate nano-sized crystal of, for example, TiN. These nanocrystals are separated from one another, and joined together, by a "tissue" of Si_3N_4 or BN or other non-metallic, covalent nitride of about one monolayer in thickness [2–4]. Several micrometer thick films of nc-M_nN/a-Si_3N_4, $(Al_{1-x}Ti_x)N$, nc-TiN/a-Si_3N_4/a- or nc-$TiSi_2$, nc-TiN/a-BN and nc-TiN/a-BN/a-TiB_2 (where M = Ti, W, V, nc = nanocrystalline, a = X-ray amorophous) nanocomposites have been shown to reach Vickers hardness of 40–100 GPa, comparable to that of diamond [2–4]. In addition to high hardness, these materials also show a high elastic recovery (upon a strain of >10%), high resistance to crack formation, high tensile strength (of 10–40 GPa, approaching the ideal strength of flow-free materials) and high thermal stability up to ≥1100 °C against coarsening and concomitant decrease of the hardness. These extraordinary mechanical properties can be reasonably well understood in terms of conventional fracture physics of nearly flow-free materials scaled down to the size of 3–5 nm [5–8].

The understanding of the mechanism of plastic deformation, and thus the origin of high hardness in these materials

* Corresponding author. Tel.: +1 510 495 2442.
E-mail address: smclark@lbl.gov (S.M. Clark).

0921-5093/$ – see front matter © 2006 Elsevier B.V. All rights reserved.
doi:10.1016/j.msea.2006.07.126

Table 1
Summary of the composition and properties of samples used for the high pressure XRD studies

Sample (composition)	[B] (at.%) (from flow)	Thickness (μm)	$H_{indent.}$ (GPa)	$E_{indent.}$ (GPa)	Cl (EDX) (at.%)	Com. stress (GPa)	Cr. size on substrate (nm)	Cr. size free standing (nm)	Random strain on substrate (%)	Random strain free standing (%)
Pro210302 (TiN-PVD)	0	10.2	26.8 ± 1.9	249	0	2.5	28.1	17.7	0.169	0.186
HF140502 (TiN-PCVD)	0	18.5	25.7 ± 2.3	256	1.74	<1.5	27	21.1	0.195	0.205
HF220702 (nc-TiN/a-BN PCVD)	5.5	9.6	30.4 ± 1.9	245	1.93	<1.5	9.7	10.8	0.500	0.459
HF230702 (nc-TiN/a-BN PCVD)	5.6	10.2	42.0 ± 2.9	311	1.18	<1.5	6.7	8.0	0.617	0.383

The PVD sample was deposited by means of reactive magnetron sputtering in N_2/Ar 1:1 mixture (mass spectrometer controlled) at total pressure of 0.002 mbar, power density at the target about 16 W/cm^2 (total 2900 W), substrate temperature = 550 °C, deposition rate = 17.2 Å/s. The PCVD samples were deposited in a high frequency (HF) discharge, 13.56 MHz, at a power of 110 W, with gas flows H_2 = 50 sccm (standard cubic centimeter per minutes), N_2 = 5 sccm, $TiCl_4$ = 1.95 sccm, power = 110 W, total pressure of 3 mbar, substrate temperature of about 590 °C and deposition rate of 0.71 nm/s.

requires more investigation. Because of the small size of the crystals dislocation activity or crystal plasticity is absent in these materials. It was therefore suggested, that, by analogy with metallic glasses, the plastic deformation occurs within the amorphous "liquid-like" tissue (Si_3N_4 or BN) by positional exchange of atoms in a way similar to the models of Deng et al. [9]. Unlike colloidal nanocrystals [10,11], the TiN nanocrystals in the superhard nanocomposites are strongly coupled via this tissue. Changes in one nanocrystallite will have an effect on those around it.

In this study, we have measured the isotropic and bi-axial strain in nc-TiN/a-BN nanocomposites prepared by plasma chemical vapor deposition (P-CVD) [4] in order to see if we can separate these effects.

2. Experimental

Samples were prepared by plasma chemical vapor deposition (P-CVD) [4] and magnetron sputtering [8] on plain steel substrates under the conditions listed in Table 1. The magnetron sputtered TiN sample was used as a reference standard for comparison with the P-CVD nanocomposite samples. All samples were characterized using: X-ray diffraction and elemental analysis and the hardness was measured using load-depth-sensing indentation. The compressive stress in the as deposited coatings was determined from the bending of the steel substrate and checked by the $\sin^2\theta$ method. The crystallite size and random strain, which are also shown in Table 1, were determined by means of the Warren–Averbach analysis in the as deposited coatings and after their removal from the substrate. Bulk modulus was measured using synchrotron X-ray diffraction to determine unit cell volume as a function of hydrostatic pressure. High pressure was generated in a diamond anvil cell (DAC), model WCME, Diacell Products Ltd. with diamonds of 300 μm culet. Gaskets of spring steel were pre-indented then drilled with a 150 μm hole. Flakes of the nanocomposite coatings of about ~30 μm in size with thickness indicated in Table 1, previously removed from their substrates, were loaded in the gasket hole along with a few chips of ruby that was used for in-situ pressure calibration [12]. Ethylcyclohexane was used as a pressure medium, which we have found to have hydrostaticity similar to that of a 4:1 methanol/ethanol mixture. A drop of ethylcyclohexane was placed in the gasket hole then the cell was sealed and pressurized. Upon sealing, the flakes of sample packed in such a way that their surfaces were parallel to the culet face of the diamonds. In our geometry, this placed the surface normal of the films parallel to the incoming X-ray beam. Large pressure gradients can exist in a diamond anvil cell especially after solidification of the hydrostatic fluid. Ethylcyclohexane solidifies at about 10 GPa. Measurements from a number of ruby chips indicated a pressure gradient across the cell of 2–3 GPa during the course of our measurements.

In-situ X-ray diffraction was conducted at the Advanced Light Source at the Lawrence Berkeley National Laboratory (Berkeley, CA), on bend-magnet beamline 7.3.3. Diffraction was collected in the angle-dispersive geometry (Fig. 1). Monochromatic X-rays were obtained from a two-bounce, channel-cut

Si(1 1 1) monochromator. The X-ray wavelength was calibrated by conducting X-ray absorption measurements on copper and germanium foils, then set to 0.8266 Å. Two-dimensional diffraction patterns were collected using a Mar345 image plate (Mar Research, Evanston, IL). The sample to detector distance was calibrated using LaB_6 and Al_2O_3 diffraction standards. Overall system accuracy was at least 0.01° in 2θ. Typical collection times were 20–30 min. Diffraction patterns were angle integrated using Fit2D [13] and fit with Voigt peak shapes. Peaks were assigned to the rocksalt structure, the stable phase of TiN. Individual peak positions were converted to d-spacings using the Bragg equation and then converted to lattice constants. Unit cell volumes were calculated by simply taking the average of the cube of the lattice constants ($V = \langle(a_0^{h\,k\,l})3\rangle$). The resulting data are listed in Table 2. After pressurization to 50 GPa the pressure was quenched to ambient. The sample was found to adhere well to the gasket after pressurization.

One annealing experiment was also conducted on sample HF140502 in order to determine the lower limit of the thermal stability of the strain induced by the high pressure. Gasket and sample were removed from the diamond anvil cell and placed in a tube oven under flowing argon at 700 °C for 2 h. A diffraction pattern was collected on the post-annealed sample using the same diffraction setup as we used for the other measurements.

3. Results and discussion

3.1. Compressibility

Fig. 2 shows the volume as a function of pressure for the three samples given in Table 2 and for pure TiN coating. No phase

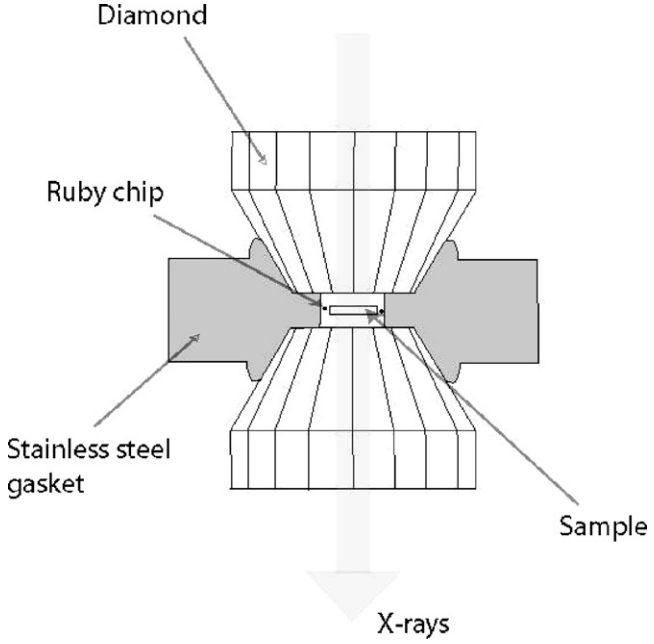

Fig. 1. Geometry of X-ray diffraction collection. The diamond anvil cell is placed with anvils perpendicular to the incident beam. Upon compression the sample films line up with the anvil faces so that the surface normal is roughly parallel to the incident beam. As such, the angle between the surface normal and the diffracted beam, Ψ, is equal to the scattering angle, 2θ.

Table 2
The unit cell volume measured at a range of pressures for each of the four samples

Pressure (GPa)	Volume (Å^3)
HF140502	
0.5	76.041
2.5	75.905
4.5	75.563
9.8	74.867
12	74.510
14.7	74.172
17.8	73.626
23.8	72.994
25.8	72.573
31.4	71.773
35.6	71.140
40.8	70.724
45.5	70.313
50.8	69.955
0	76.785
HF220702	
1.2	78.042
2.7	77.415
3.4	77.353
5.8	76.852
7.8	76.381
9.2	75.940
19.8	74.054
21.4	73.882
25.1	73.112
27.3	72.273
29	72.157
32.1	71.523
34.2	71.212
40	69.044
44	68.764
49	68.564
0.2	77.864
HF230702	
3.5	77.117
5.2	76.763
7.8	76.421
11.2	75.837
14.1	75.372
17.2	74.865
20.1	74.865
20.1	74.440
23.2	73.944
26	73.705
35.8	72.053
40.9	71.202
46.1	70.748
51.2	70.107
0	77.192
Pro210302	
0.1	76.620
1.1	76.380
2.2	76.212
4.5	75.785
6.3	75.284
9.2	74.765
12.6	74.167
13.8	74.016
16	73.481
18.5	73.066

Table 2 (*Continued*)

Pressure (GPa)	Volume (Å^3)
22.9	72.643
25.5	72.180
28.9	71.733
32.3	71.041
36.6	71.254
40.2	70.436
47	69.215

These results are plotted in Fig. 2.

transition was observed and all the samples retained their cubic structure. The compressibility of the nano-structured and the TiN samples are very similar (Table 2 and Fig. 2). The nc-TiN/a-BN nanocomposite samples HF220702 and HF230702, that contains the a-BN tissue, have a noticeably larger V_0 than pure TiN deposited by P-CVD (sample HF 140502) or by reactive sputtering (sample Pro 220202), but the two $V(P)$ curves parallel one another very well up to about 20 GPa. Above 20 GPa, the compressibility of HF220702 (nc-TiN/a-BN with a hardness of only 30 GPa due to a non-optimum BN tissue) seems to increase, but that of the other samples remains essentially the same as before.

The somewhat larger V_0 found for the nc-TiN/a-BN nanocomposites is due most probably to the tensile stress that is a result of incoherency strain, or lattice mismatch, between the TiN and BN phases, the latter having a much smaller average size of the atoms (B versus Ti) [4,8]. Interestingly, sample HF230702 which has the highest hardness of 42 GPa retains its excess volume of the TiN unit cell up to the highest pressures used here whereas V_0 of sample HF220702, whose BN-tissue is far from the optimum ($H \approx 30$ GPa, see [4]), decreases to that of TiN at pressures $\geq$25 GPa. At higher pressures, the scattering of the data increases. However, one should keep in mind that the unit cell volume is calculated from the averages of the lattice constants obtained from all five ($h\,k\,l$) Bragg reflections.

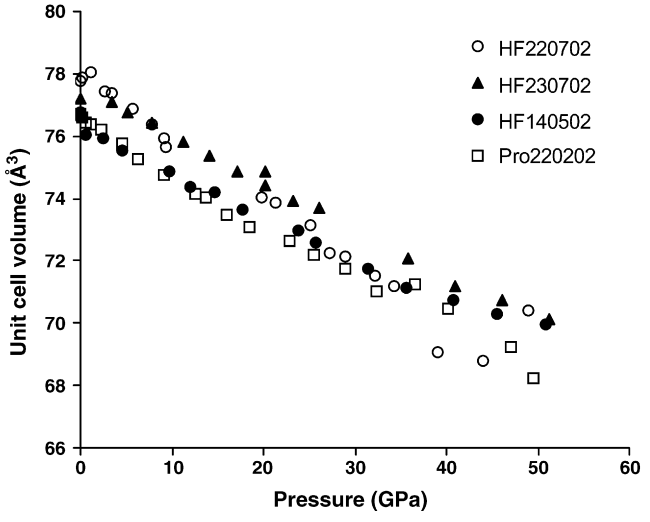

Fig. 2. Volume as a function of pressure for three nanocomposite samples deposited by plasma CVD and one sample of pure TiN prepared by reactive sputtering (Pro210302). The compressibility differences between the samples cannot account for the elevated hardness of these materials.

Because there is a wide dispersion in the values of $a_0^{h\,k\,l}$ (particularly at higher pressures, see below), the deviations in volume at $\geq$25 GPa may be due in no small part to strain.

3.2. Biaxial strain

3.2.1. Experimental results

The value of the lattice constant was found to have a much greater spread than the resolution of the system. The lattice constants derived from each ($h\,k\,l$) reflection by using the Bragg equation are presented in Fig. 3 for all four samples studied. The difference between the values is fairly large, in particular for the nc-TiN/a-BN nanocomposites (see Fig. 3b and c). This difference decreases for the TiN sample at smaller pressure (Fig. 3a and d). While this phenomenon has been observed before in TiN films at ambient pressure [14–16], differences of about 0.01 Å are more typical. Only the least strained TiN samples HF140502 deposited by P-CVD (Fig. 3a) and Pro210302 deposited by reactive sputtering (Fig. 3d) have, at the low pressure, such small differences in the $d(h\,k\,l)$ values. The nc-TiN/a-BN nanocomposites HF220702 and HF230702 with the highest hardness of 30.4 and 42.0 GPa, respectively, show both higher $d(h\,k\,l)$ values and greater difference among different $h\,k\,l$ even at zero pressure, possibly due to the above mentioned incoherency strain. Sample HF230702 with the highest hardness has the largest difference of approximately 0.06 Å. The difference among the $d(h\,k\,l)$ values increases with increasing pressure for all samples studied here with the lattice parameter calculated from the (1 1 1) Bragg reflection being largest.

This type of difference in lattice parameters calculated from different ($h\,k\,l$) reflections was reported for TiN thin films by Rafaja et al. [16] and interpreted as the results of biaxial stress in the plane of the film adhering to a substrate and zero stress in normal direction in combination with anisotropy of the stiffness (Young's modulus) of the TiN lattice. Generally, the biaxial strain in thin films is analyzed by taking diffraction patterns at different values of Ψ, the angle between the diffracted X-ray beam and the surface normal. This analysis of the strain is associated with a number of difficulties, and is not possible in our geometry, because the angle Ψ is restricted to $\Psi = 2\theta$. Nevertheless, the analysis presented below gives a consistent picture.

3.2.2. Fit to model

In order to better understand the origin of the differences in the strain obtained from different ($h\,k\,l$), reflections as found in the samples of the films studied here, which were removed from the substrate prior to the HP XRD measurements, the data for the least strained TiN coating deposited by P CVD (HF140502) were fitted using the model of Rafaja et al. [13]. This model assumes a restricted relaxation of the lattice in the plane of the film parallel to the substrate surface due to its adhesion and allowed expansion in the direction normal to the surface. Furthermore, the model takes into account that TiN is most easily deformable in the ⟨1 1 1⟩ direction (the values of elastic moduli are directionally dependent in cubic crystals [14]). This then gives the magnitude of the lateral strain and the strain free lattice constant.

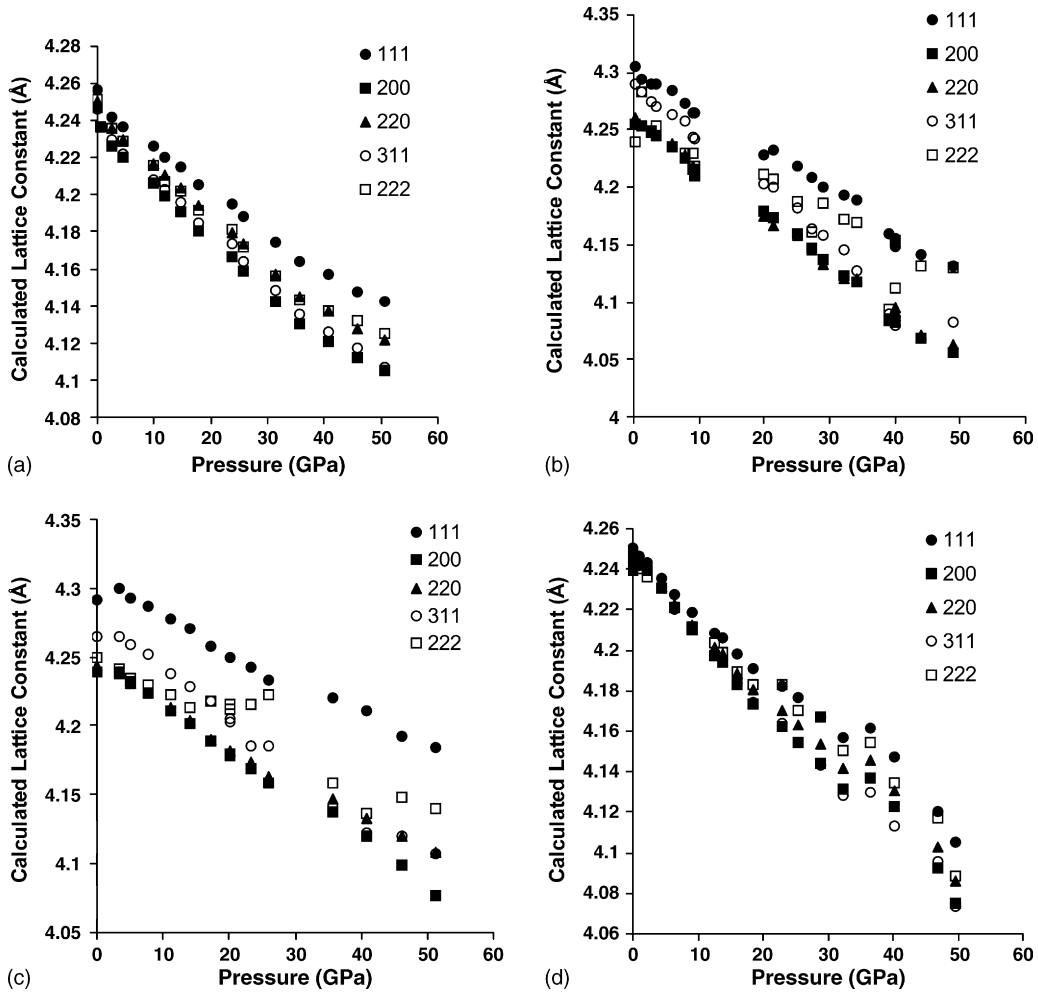

Fig. 3. Lattice constants derived from each $h\,k\,l$ peak as a function of pressure for four samples, (a) TiN deposited by plasma CVD HF140502, two nc-TiN/a-BN nanocomposites coatings deposited by plasma CVD, (b) HF230702, (c) HF220702, and (d) TiN deposited by reactive sputtering Pro210302.

The results of the fits to the Rafaja's model are presented in Figs. 4 and 5. Fig. 4 shows the difference between observed and calculated values of the lattice constants as a function of 2θ for two pressures, 2.5 GPa (Fig. 4a) and 50.8 GPa (Fig. 4b). The agreement is reasonably good and reproduces the trend of ($h\,k\,l$) peaks.

Fig. 5a shows the values of lateral strain determined using the model of Rafaja [16]. It can be seen that the strain increases

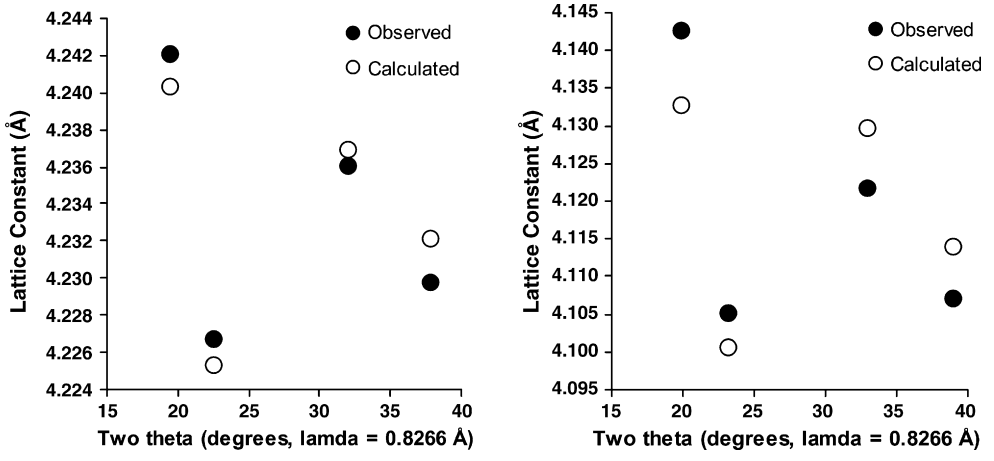

Fig. 4. Comparison of observed (full symbols) and calculated (open symbols) lattice constants for patterns taken at (a) 2.5 GPa and (b) 50.8 GPa.

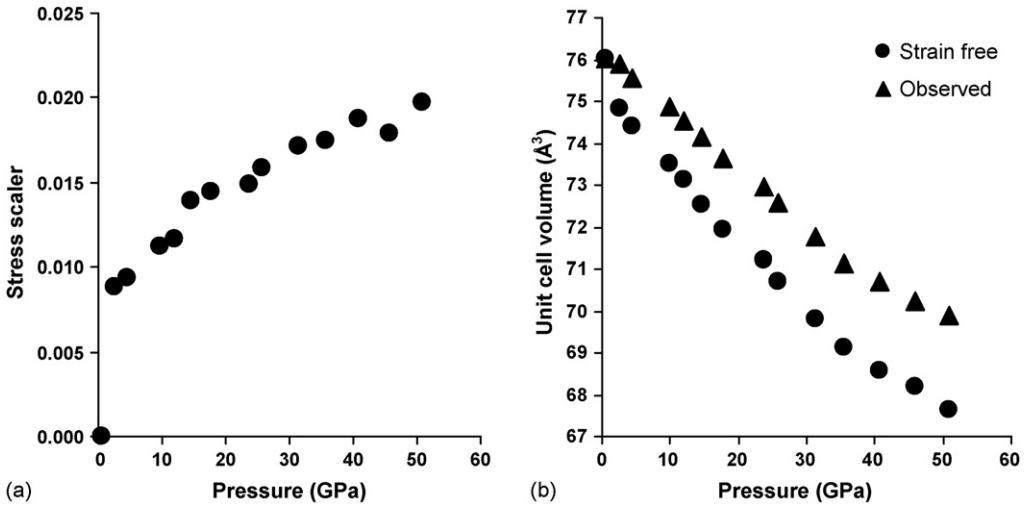

Fig. 5. Results of model analysis. The lateral strain, Δp (a) and the zero-strain lattice volumes (b) are shown as a function of pressure.

markedly between the lowest pressure of 0.1 GPa used and the second one of 2.5 GPa. Above this pressure the strain increases more or less monotonically up to the highest pressure obtained.

Fig. 5b shows the unit cell volume $= \langle (a_0^{\text{strainfree}})^3 \rangle$ as a function of pressure. Both the observed volumes and the volumes corrected for strain are shown.

The finding that the model of Rafaja soundly fits the data implies that the model takes into account the major phenomena present in these systems, a strong radial strain due to the radial pressure gradients within the diamond cell and its bi-axial relaxation coupled with the deformation being largest in the $\langle 1\,1\,1 \rangle$ direction. The large amount of dispersion between lattice constants from each $h\,k\,l$ is indicative of the large role played by the easy deformation direction of the material in the amount of bi-axial strain observed. The strain in the films increases with pressure. This implies that the internal strain of the material is converting the hydrostatic pressure in the cell into directional stress within the film as schematically illustrated in Fig. 6.

The compressive stress due to the radial pressure gradient creates a tensile strain in the perpendicular direction which causes anisotropy similar to that observed by Rafaja et al. [16].

Tensile strain in the direction normal to the plane of the film affects the observed volume [17]. As can be seen in Fig. 5b, the presence of the strain has the effect of making the materials less compressible. Rather than all of the PV work going into the reduction of the volume, some is being redirected into producing anisotropic strain in the film.

3.3. Isotropic (random) strain

All samples showed increases in the width of the Bragg reflections after quenching to ambient pressure. Table 3 shows the results of an analysis using the Warren–Averbach method [18]. The results show that the random strain after pressurization increases for all samples. However, the amount of this increase decreases with increasing hardness when the stable nanocomposite structure is formed as illustrated by Fig. 7. This is an important finding that illustrates clearly the increase of the resistance of the TiN containing coatings against deformation by the formation of a stable nc-TiN/a-BN nanocomposite. The a-BN tissue evidently carries the largest part of the reversible, albeit non-linear elastic, deformation by flexing as suggested by us recently [6]. Because this tissue is formed by the self-organization upon the spinodal phase segregation, it is almost free of build-in flaws and, therefore, the tensile strength of these nanocomposites of 10–40 GPa approaches the ideal strength $\sigma \approx (\gamma_S E_Y / a_0)^{0.5}$ of strong materials (here γ_S is the surface energy, E_Y is the Young's modulus and a_0 is the equilibrium interatomic distance) [5–7].

Strain induced in TiN during the deposition e.g. by energetic ion bombardment has been reported in these systems earlier and it can be relieved by annealing to 400–600 °C. Therefore, we studied the annealing behavior of the deformation in the TiN coating deposited by plasma CVD which showed the largest increase of strain after it has been subjected to high pressure in the diamond cell. For this purpose, sample HF140502 was recovered in its gasket from the DAC after pressurization and heated to 700 °C for 2 h. X-ray diffraction was then collected on this annealed sample. Fig. 8 shows the results of this experiment. The diffraction patterns of the post-pressurization and the subsequently annealed samples are nearly identical in peak width and intensity. The finding that the random strain in the TiN crystallites of the pure TiN film persists the 2 h anneal-

Table 3
Results of Warren–Averbach analysis of line-broadening for samples before and after pressurization

Sample	Random strain, pre-pressurization (%)	Random strain, post-pressurization (%)
HF140502	3.4	7.7
HF220702	3.3	6.3
HF230702	9.3	10.2
Pro	2.9	6.5

All samples demonstrate significant increases in strain post-pressurization.

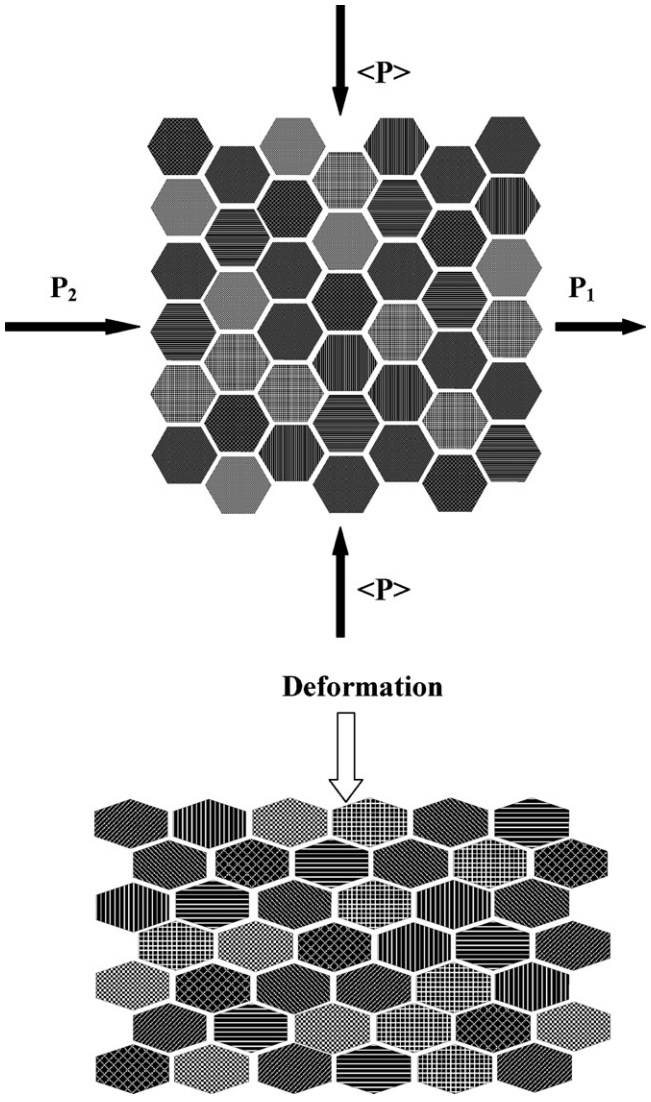

Fig. 6. Schematic illustration of the plastic flow of the nanocomposites as result of the radial pressure gradient (from the left to right in the figure) in the diamond cell. The grain boundary sliding results in a permanent plastic deformation which causes elastic deformation of the randomly oriented TiN nanocrystals thus giving rise to the additional random strain.

ing to 700 °C indicates that some bonds were broken and others formed, implying some type of plastic deformation. Plastic deformation is unlikely to occur within the small TiN nanocrystals, because due to the lack of dislocation activity their strength reaches the ideal shear strength of about 10% of the shear modulus. Van Vliet et al. have recently shown that upon nanoindentation into soft metallic single crystals the first plastic events occurs within a critical volume of a linear dimension of about several 10 nm [19]. Therefore, in pure TiN films the increase of the random strain of the TiN nanocrystals is most probably due to their elastic deformation associated with an irreversible grain boundary sliding. Upon the formation of the nc-TiN/a-BN nanocomposite the strong BN (or Si_3N_4) interfacial monolayder avoids the grain boundary sliding and, consequently, the formation of strain within the TiN crystallites that should be of an elastic nature. Because the nanocrystalls are randomly oriented within the nanocomposites, the bi-axial deformation of the flakes

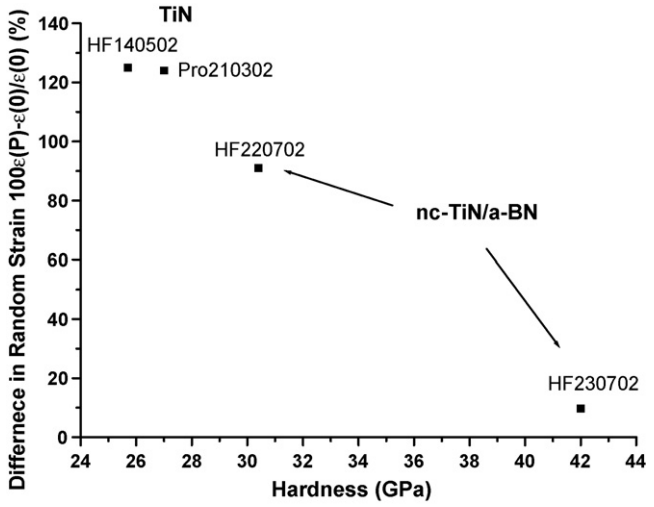

Fig. 7. Difference in random strain after pressurization to 50 GPa vs. the hardness of the coatings.

of the nanocomposites results in the random (isotropic) strain as illustrated in Fig. 6.

3.4. Reduction of the volume after decompression

Within the accuracy of the measurements, the volume after decompression returns to the original value for the TiN samples Pro210302 and HF140502 (see Table 2 and Fig. 2). However, for the harder nc-TiN/a-BN samples HF220702 and HF230702, a small but unambiguous decrease of the zero pressure volume of about 0.4 ± 0.2 and 0.8 ± 0.2 Å^3, respectively, after the decompression can be seen. This can be due either to a diffusion of boron, interstitially dissolved within the BN nanocrystals, into the grain boundaries, or to the densification of the incoherent TiN/BN interface which is, in the as deposited films, under tensile strain (see Fig. 12a in Ref. [20] and related discussion therein). Because the films were deposited under conditions where immiscible, stoichiometric TiN and BN nitrides

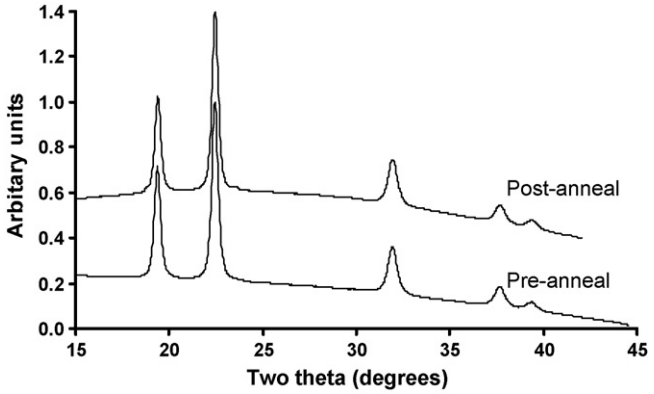

Fig. 8. X-ray diffraction of HF140502 samples, both post-pressurization and quenched to ambient pressure. The diffraction pattern of the sample which has been annealed for 2 h at 700 °C was shifted upwards for clarity. The lack of any change in the widths of the peaks implies that strain has not been relieved by annealing.

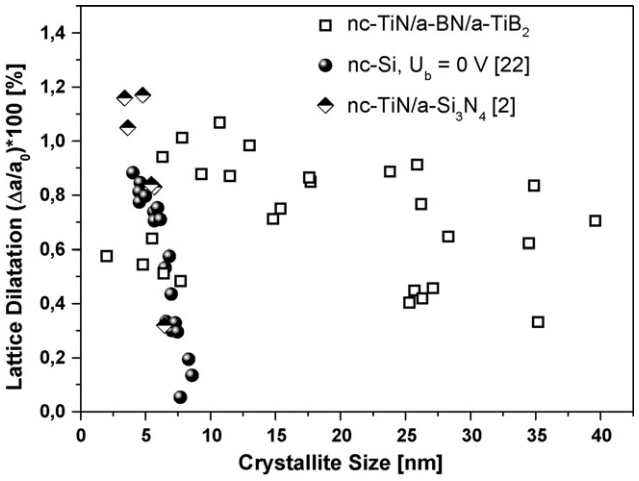

Fig. 9. Dependence of the lattice dilatation ($\Delta a/a_0$) on the crystallite size of nc-TiN/a-BN/a-TiB_2, nc-Si [22] and nc-TiN/a-Si_3N_4 [2] coatings. The decrease of the dilatation for the ≤7 nm small TiN nanocrystals is due to the formation of a large fraction of a-TiB in coatings with a large fraction of boron of ≥10 at.% (see [20,21]).

are formed and the temperature was high enough to allow for a sufficiently fast diffusion during the deposition which is needed for the system to reach equilibrium [8,20], the possibility of the formation of interstitial boron and its diffusion from the TiN nanocrystals into the grain boundaries is ruled out, and the densification of the grain boundaries is considered as the most likely process.

Indeed, observing the locally pseudomorph structure of the interfacial monolayer of BN between the TiN nanocrystals with a relatively large excess free volume (see Fig. 12a in Ref. [20]), where the maximum hardness is achieved (see Fig. 7 in [20]), it is clear that the TiN nanocrystals are subject to a large tensile strain causing their dilatational elastic deformation as shown in Fig. 9 which was taken from Ref. [21]. The decrease of the dilatation for the ≤7 nm small TiN nanocrystals, which is seen in Fig. 9, is due to the formation of a large fraction of a-TiB_2 which relaxes the tensile strain caused by the BN (see [20,21]). The TiB_2 phase appears in these nanocomposites only at a relatively high boron content of about ≥10 at.% [20,21]. In the present paper we investigated only materials with a relatively small amount of boron of <6 at.%, where the fraction of the TiB_2 phase is negligible and the tensile strain large (see Fig. 9, data for crystallite size ≥10 nm).

The lattice dilatation due to the tensile strain within the grain boundaries is more pronounced for the TiN/BN system as compared with the nc-Si [22] and nc-TiN/a-Si_3N_4 [2], and it persist at much larger grain size. We refer to papers [2], [21] and [22] for further experimental details and discussion. Significant elastic stiffening and increase resistance against plastic deformation of the superhard nanocomposites due to pressure-enhanced elastic moduli upon indentation was elaborated in our recent paper [23]. The densification of the grain boundaries of the nc-TiN/a-BN nanocomposites after the pressurization, as found in the present paper, is likely to result in an additional increase of their stiffness. This may be investigated, e.g. by careful indentation experiments in the future.

4. Conclusions

We have shown that, as in the case of the nc-TiN/a-Si_3N_4 nanocomposites, the compressibility of the nc-TiN/a-BN nanocomposite materials is not significantly different from that of pure TiN. This implies that the nanocomposite materials derive their strength from their composite structure rather than from an alteration of the interatomic potential.

Under hydrostatic pressure increasing from 0 up to 50 GPa, a large amount of strain is formed in pure TiN and in the nc-TiN/a-BN nanocomposites. Both directional (biaxial) and isotropic (random) strain are present. After pressurization and quenching to zero pressure, the random, isotropic strain persists. The relative increase in random strain after pressurization is inversely proportional to the hardness of the original thin film.

In pure TiN, where the residual post-pressurization strain is largest and, therefore, could be measured more accurately, this strain persists even after annealing to 700 °C for 2 h. This indicates that the TiN films undergo some kind of permanent deformation at high pressure. Because crystal plasticity (plastic deformation by the multiplication and movement of dislocations) requires a minimum critical volume within which a dislocation multiplication source can operate (typically corresponding to a linear size of the order of 10 nm (see [3,5,6,8,24] and references therein)), the permanent deformation observed in the TiN films must be localized within the grain boundaries (grain boundary sliding). This deformation at the grain boundaries provides the stress field for elastic deformation of the TiN nanocrystals that is seen by XRD. This deformation is highly resistant to thermal annealing because of the irreversible nature of the grain boundary sliding.

Upon the formation of nc-TiN/a-BN superhard nanocomposites that have a strong TiN/BN interface and are stable up to ≥950 °C, the a-BN tissue prevents the plastic deformation within the grain boundaries. This is seen in the decrease of the difference in the random strain after and prior to the pressurization. It will be interesting to perform similar studies on the nc-TiN/a-Si_3N_4 nanocomposites because the semi-coherent TiN/Si_3N_4 interface has much smaller stress due to a smaller difference between the size of Ti and Si atoms [8].

Reduction of the zero-pressure volume is observed after the decompression for the nc-TiN/a-BN nanocomposites but not for the TiN. This is explained by densification of the one monolayer BN interfacial layer under the high pressure.

Acknowledgements

This work was supported by the Director, Office of Science, Office of Basic Energy Sciences, Division of Materials Sciences and Engineering, of the U.S. Department of Energy under Contract No. DE-AC03-76SF00098, and by the Air Force Office of Scientific Research, Air Force Material Command, USAF, under grant number F49620-01-1-0033. The Advanced Light Source is also supported by U.S. Department of Energy under Contract No. DE-AC03-76SF00098. The work on the development, preparation and characterization of the superhard nanocomposites was supported by the European Commission

6th Framework Programme under Contract No. AST 3-CT-2003-502741—"MACHERENA" and Contract No. CA 505549-1—"DESHNAF". We thank Dr. J. Prochazka for the deposition of the reference TiN coatings by reactive magnetron sputtering.

References

[1] J.J. Gilman, Mater. Sci. Eng. A 209 (1996) 74.
[2] S. Veprek, S. Reiprich, L. Shizhi, Appl. Phys. Lett. 66 (1995) 2640.
[3] S. Veprek, J. Vac. Sci. Technol. 17 (1999) 2401.
[4] P. Karvankova, M.G.J. Veprek-Heijman, O. Zindulka, S. Veprek, Surf. Coat. Technol. 163/164 (2002) 149.
[5] A.S. Argon, S. Veprek, MRS Symp. Proc. 697 (2002) 3.
[6] S. Veprek, A.S. Argon, J. Vac. Sci. Technol. B 20 (2002) 650.
[7] S. Veprek, S. Mukherjee, P. Karvankova, H.-D. Männling, J.L. He, K. Moto, J. Prochazka, A.S. Argon, J. Vac. Sci. Technol. A 21 (2003) 532.
[8] S. Veprek, M.G.J. Veprek-Heijman, P. Karvankova, J. Prochazka, Thin Solid Films 476 (2005) 1.
[9] D. Deng, A.S. Argon, S. Yip, Phil. Trans. Royal Soc. (London) 329 (1989) 614.
[10] S.H. Tolbert, A.P. Alivisatos, Science 265 (1994) 373.
[11] J.N. Wickham, A.B. Herhold, A.P. Alivisatos, Phys. Rev. Lett. 84 (2000) 923.
[12] M. Eremets, High Pressure Experimetal Methods, Oxford University Press, Oxford, 1996.
[13] A.P. Hammersley, S.O. Svensson, M. Hanfland, A.N. Fitch, D. Husermann, High Pressure Res. 14 (1996) 235.
[14] V. Valvoda, J. Alloys Compd. 219 (1995) 83.
[15] R. Kuzel, R. Cerny, V. Valvola, M. Blomberg, M. Merisalo, S. Kadlec, Thin Solid Films 268 (1995) 72.
[16] D. Rafaja, V. Valvoda, R. Kuzel, A.J. Perry, J.R. Treglio, Surf. Coat. Technol. 86/87 (1996) 302.
[17] J.F. Nye, Physical Properties of Crystals, Their Representation by Tensors and Matrices, Oxford University Press, Oxford, 1985.
[18] H.P. Klug, L.E. Alexander, X-ray Diffraction Procedures, 2nd ed., John Wiley, New York, 1974.
[19] K.J. Van Vliet, J. Li, T. Zhu, S. Yip, S. Suresh, Phys. Rev. B 67 (2003) 104105.
[20] P. Karvankova, M.G.J. Veprek-Heijman, D. Azinovi'c, S. Veprek, Surf. Coat. Technol. 200 (2006) 2978.
[21] P. Karvankova, Ph.D. Thesis, Technical University, Munich, 2003, available upon: (http://tumb1.biblio.tu-muenchen.de/publ/diss/ch/2003/karvankova.pdf).
[22] S. Veprek, Z. Iqbal, F.A. Sarott, Phil. Magn. B 45 (1982) 137.
[23] R.G. Veprek, D.M. Parks, A.S. Argon, S. Veprek, Mater. Sci. Eng. A 422 (2006) 205.
[24] J.S. Koehler, Phys. Rev. B 2 (1970) 547.